J Mater Sci (2015) 50:7126–7136
DOI 10.1007/s10853-015-9269-5

A combined X-ray absorption spectroscopy and molecular dynamic simulation to study the local structure potassium ion in hydrated montmorillonite

Visit Vao-soongnern[1] · Chinnawut Pipatpanukul[1] · Suksun Horpibulsuk[2]

Received: 29 April 2015 / Accepted: 14 July 2015 / Published online: 21 July 2015

Abstract Atomistic local structure of potassium ion adsorbed in hydrated montmorillonite (MMT) was investigated based on a combination of an extended X-ray absorption fine structure (EXAFS) spectroscopy and classical molecular dynamics (MD) simulation. The accuracy of the representative MMT atomistic model with PCFF-INTERFACE force field was validated. MD-simulated EXAFS spectra were calculated from trajectories of hydrated MMT atomic coordinates and the results were in satisfactory agreement with corresponding experimental EXAFS spectra. Interlayer spacing determined by X-ray diffraction was consistent with the mono-layer hydrated MMT structure. The first coordination shell of K^+ ion in monohydrated MMT was formed by 5 water oxygen atoms at an average $K–O_W$ distance of 2.85 Å and the second coordination shell of 6 oxygen atoms from both sides of the closest silicate tetrahedral sheet at $K–O_{MMT} = 3.41$ Å. For hydrated K^+-MMT, MD and EXAFS results confirm that K^+ counter ions form the inner-sphere surface complex and that the adsorbed sites were located with the vicinity edge of a basal oxygen hexagonal cavity in the silicate tetrahedral sheets of MMT. For higher-layer hydrated MMT, K^+ ions can form surface complexes that are inner-sphere, outer-sphere, and transient diffuse-layer species depending on the number of intercalated water in the clay. Water molecules are of less ordered arrangement in the monohydrated MMT due to the confinement effect from the clay surface. K^+ counter ions in the single layer hydrates are almost trapped within the cavities of the basal planes surface.

✉ Visit Vao-soongnern
visit@sut.ac.th

[1] School of Chemistry, Institute of Science, Suranaree University of Technology, Nakhon Ratchasima 30000, Thailand

[2] School of Civil Engineering, Institute of Engineering, Suranaree University of Technology, Nakhon Ratchasima 30000, Thailand

Introduction

The structure and surface geochemistry of clay minerals are important to understand some of the basic features of their properties. Montmorillonite (MMT) is among the most common clay minerals and has received much attention owing to its physical and chemical properties. MMT is important in a number of technological and industrial applications such as catalytic activity, adsorbents in environmental engineering, waste disposal, polymer nanocomposites, and biotechnology (sensors, wound dressings) [1–5]. Many applications of MMTare related to its ability to interact with ions and water. For our interest, we plan to employ MMT as the filler for geopolymer synthesized from fly ash activated by KOH solution. Geopolymer cement is an innovative material and a real alternative to conventional Portland cement which has the potential to be used in civil engineering applications such as for use in transportation infrastructure, construction, and offshore applications [6].

MMT is a subclass of smectite, a 2:1 tetrahedral-octahedral-tetrahedral (TOT) type of phyllosilicate mineral consisting of two tetrahedral sheets separated by one octahedral sheet. It is characterized as having greater than 50 % octahedral charge; its cation exchange capacity (CEC) is due to isomorphous substitution of Mg for Al in a central octahedral sheet making the clay platelets negatively charged, which are compensated by interlayer cations. The interlayer space of TOT clay mineral is the

space between two parallel silicate sheets, sandwiched by two oxygen planes of siloxane group. At the same time, the capacity of MMT to incorporate water into its interlayer region and cause clay swelling is of central interest. The clay swelling is the interlayer space resulting from (a) the thermal motion of water in an environment of the mineral, (b) the electrostatic attraction forces between the molecules and the exchangeable cationic species, and (c) the attraction and the dispersion forces between TOT sheets significant uptake of water content which causes expansion of the clay crystal along the c axis (which defines the direction between two parallel silicate layers of clay). The water content of MMT is variable and it increases greatly in volume when it absorbs water. Chemically, it is hydrated sodium calcium aluminum magnesium silicate hydroxide $(Na,Ca)_{0.33}(Al,Mg)_2(Si_4O_{10})(OH)_2{\cdot}nH_2O$. Potassium, iron, and other cations are common substitutes, the exact ratio of cations varies with source [7–10].

Structural characterization of MMT at the atomistic level is difficult as this mineral is not a well-defined crystal structure that prevents the study by conventional diffraction methods. Nevertheless, some fundamental studies based on an extended X-ray absorption fine structure (EXAFS) spectroscopy have been applied to investigate the detailed solvation structure of ionic solution [11–19] and ions adsorbed in clay. EXAFS analyses require a structural model around an adsorbed ion in order to determine the site where ions are adsorbed on the clay surface. For example, determination of structural information of Cr^{3+}, U^{6+}, Ni^{2+}, Sr^{2+}, Zn^{2+}, Ba^{2+}, Cu^{2+}, Cs^{1+}, and others in clays has been reported [20–27]. In addition to this experimental investigation, molecular simulation such as Monte Carlo (MC) and molecular dynamics (MD) is also an alternative way to gain an insight at an atomistic level for the structure and dynamics of ions in solution and in hydrated clay minerals [28–32], in particular, an interest in the swelling of MMT clays and hydration of their interlayer cations. The reliability of MD or MC results is based on a correct description of a force field representing interactions between atoms.

Recently, the combination of MD simulation and EXAFS experiment—so called MD-EXAFS, a method to generate EXAFS spectra to determine the local atomistic structure of the probed atom/ion from an MD simulation, has been developed. Due to the advancement of modern EXAFS algorithms and the availability of more accurate ion and solvent potential models, the number of studies that combine MD with EXAFS has increased considerably [33–40]. MD-EXAFS has been successfully used by our research group to study the solvated ion in the amorphous portion of polymer/salt complexes [41–43]. MD-EXAFS spectra were generated from MD simulation and there was a remarkable consistence between calculated and measured MD-EXAFS spectra. Information on the atomistic local structure around the probed ion can be precisely obtained from this MD-EXAFS technique.

In this work, we are interested in extending the combination of MD and EXAFS techniques to study the local structure of the potassium ion hydrated montmorillonite (K^+-MMT). The main objectives of this study are (a) to apply both EXAFS experiment and MD simulation to determine the atomistic scale for the local structure of the adsorbed K^+ ions in hydrated MMT and (b) to investigate the behavior of interlayer species residing on the solid-water interface in MMT hydrates.

EXAFS spectroscopy

Background of EXAFS

EXAFS spectroscopy is a method widely used for characterization of local structure of the probed atom. In EXAFS, an X-ray source is tuned to energies just slightly above an inner-shell electron absorption edge. As a result, a low-energy electron is ejected and is back-scattered by atoms of the nearest solvent shells. This scattering process leads to interferences with the outgoing wave, giving rise to the characteristic oscillations of the EXAFS spectra. EXAFS spectra and molecular structure can be determined by the evaluation of electron scattering analysis [11–14]. In standard EXAFS analysis, the fine structure factor is defined by

$$\chi(E) = \frac{\mu(E) - \mu_0(E)}{\Delta\mu_0(E_0)}, \tag{1}$$

where $\mu(E)$ is the absorption coefficient as a function of the X-ray energy E, $\mu_0(E)$ is the background absorption coefficient, and $\Delta\mu_0(E_0)$ is the jump in the absorption background at the absorption edge, E_0. Given a set of neighboring atoms located at positions r_i relative to the photoelectron source located at r_0, with $R_i = |r_i - r_0|$, the EXAFS signal in k-space is described by

$$\chi(k) = \sum_i N_i \frac{F_i(k)}{kR_i^2} e^{-2\sigma_i^2 k^2} e^{-2R_i/\lambda} \sin[2kR_i + \phi_i(k)] \tag{2}$$

where the photoelectron wave-vector, k, is related to the X-ray energy by $E = E_0 + (\hbar^2 k^2)/2m_e$. N_i is the number of neighboring atoms in the ith coordination shell at a distance R_i away from the absorbing atom. The backscattering amplitude and mean-squared displacement of the neighboring atoms are given by $F_i(k)$ and σ_i, respectively. The phase shift of the photoelectron is given by $\varphi_i(k)$, while the exponential term containing the mean free path λ of the photoelectron accounts for their inelastic scattering. It is this exponential damping term which accounts for the selectivity of EXAFS to short-ranged order. The backscattering amplitude and the phase shift functions are extracted

from EXAFS spectra taken from a standard which has a known structure and which contains the same absorbing and scattering elements as the unknown. A Fourier transform of the oscillations in k-space yields a real-space distribution, similar to a radial distribution function (RDF). Fitting Eq. (2) to the measured EXAFS spectra can provide the structural parameters: the number and type of surrounding atoms, their average distance to the central absorbing atom, and their distribution about the absorbing center.

Experiments

Materials

Na-montmorillonite (Swy-2) was obtained from the Source Clay Repository of the Clay Mineral Society. In general, the Swy-2 source clay is at the lower end of CEC = 65–100 -meq/100 g. (CEC of 76.4 meq/100 g was reported in the repository homepage at www.clays.org) Ion exchange clay samples were prepared by adding 4 ml of 0.1 M KCl solution to 2 g of a dried weight of suspended Na^+-MMT in 196 ml of water. The pH of suspension was adjusted to pH 7 with 0.1 M NaOH solution and 0.1 M HCl solution. The clay was washed with deionized water and centrifuged to separate sediment and to remove residue; the wet pastes were washed once with deionized water and dried in vacuum oven at 80 °C for 24 h. The sample was kept in desiccator before performing X-ray diffraction experiment to determine the interlayer spacing. The same samples were used for EXAFS measurements on the same date to ensure the same condition of MMT used in this work.

EXAFS data collection and processing

X-ray absorption spectra were collected in the fluorescence mode at the Potassium K-edge at the Synchrotron Light Research Institute (SLRI), Nakhon Ratchasima, Thailand. The samples were measured using a Lytle fluorescence detector at room temperature. Si (111) monochromators were used for all samples. The monochromator was detuned 50 % at the highest energy of the scan to minimize the contribution from higher-order harmonics. At E_0 of 3608.4 eV, 1-eV steps were used in the pre-edge region, while 0.2-eV steps were employed from 60 eV below the edge to 60 eV above the edge. For the EXAFS region (60 eV above the edge to 800 eV), 1-eV steps were employed. Energy calibration was performed by KI salt for all samples. The K-edge absorption was detected using an ionization chamber filled with He and Ar for the incident intensity measurement. A total of 3 scans were collected, and these scans were added after E_0 determination before further data analysis to improve the signal-to-noise ratio.

The EXAFS data were processed using ATHENA software package [18]. For each sample, the collected spectra were averaged and the background absorption was subtracted by fitting a straight line through the pre-edge-region. After normalization, the absorption data were converted from energy to k-space and then these spectra were weighted by k^2 to compensate for damping of oscillation at high k.

Molecular dynamic (MD) simulation

The model and force field

MMT model was obtained by isomorphous substitutions of trivalent Al atoms of the octahedral sites by divalent Mg atoms and tetravalent Si by trivalent Al atoms. The unit cell formula was given by $K_{0.333}nH_2O$ $(Si_4O_8)(Al_{1.667}Mg_{0.333}O_2)(OH)_2$. The basic cubic cell contained 1220 atoms of 720 O, 240 Si, 100 Al, 20 Mg, 120 H, and 20 K^+ ions. The MMT model was generated using the optimized PCFF-INTERFACE force field developed by Heinz et al. [44, 45] for the layer silicates take surface energies accurately into account, and thus reproduce crystal structures, surface energies, and approximate vibrational frequencies of phyllosilicates in good agreement with experiment. MMT structures were considered with CEC of 91 mequiv/100 g which is in the range of the swy-2 source clay (65–100 meq/100 g) sample used in this experiment. Each X and Y sides are 25.59 Å and Z is 27.05 Å slab of interlayer spacing. Periodic boundary conditions were applied on three space direction.

We used the simple point charge water model, which is one of the most accurate three-center water models without taking into account the polarization. Three-site models have three interaction points corresponding to the three atoms of the water molecule. Each site has a point charge, and the site corresponding to the oxygen atom also has the Lennard-Jones parameters (the partial charge: $\delta_H = +0.40$, $\delta_O = -0.80$ with an averaged bond length: $l_{O-H} = 1.02$ Å).

MD simulation

K^+-MMT structure models were generated in periodic boundary condition. First, the generated structures were equilibrated by performing energy minimization by both steepest descent and conjugated gradient methods. Then *NPT*-MD simulation was simulated at 300 K and 0.1 MPa under the assumption that two layers of 2:1 sheets and two layers of interlayer extended infinitely to a horizontal direction. The equations of motion were integrated using the velocity Verlet algorithm with a time step of 1 fs. Simulation was performed for about 10^6 steps using 1 fs per step to determine the structural properties at equilibrium.

Second, *NVT*-MD simulation was run for another 10^6 steps at 300 K and it was used for later data analysis. We also simulated K^+ ion in aqueous solution in order to compare the local salvation structure with the hydrated K^+-MMT model. The aqueous solution consists of one K^+ ion and 150 water molecules in a cubic simulation box with cell length determined from the density of 1.0 g/cm^3. After minimization, the ion–solvent systems were equilibrated for 100 ps followed by a 1 ns MD trajectory for data analysis. In each system, three independent initial structures were performed for the MD simulation to improve the statistics of the calculated results. Interlayer spacing of clay swelling as a function of loaded water molecules was also determined by the NPT-MD simulation. After a trial change of particle position, a box change was tried in such a way that the stress normal to the surface of the MMT with pressure was kept constant. For this target, the box fluctuations were allowed only in the Z-direction. All MD simulations were performed using the Discover module in Materials Studio 4.2 provided by National Nanotechnology Center, Thailand.

MD-EXAFS

Simulated MD-EXAFS spectra were computed by the selected 100 independent configurations of water molecules and MMT atoms surrounded K^+ ions from three independent runs of 1-ns MD trajectories. For each configuration, a cluster of the closest water molecules and MMT atoms of the photoelectron source (K^+ ion in aqueous solution and hydrated MMT) were extracted from the configuration to form the coordinate input for electron multiple scattering analysis. This forms a cluster surrounding the probed ion with a radius of 6 Å (this cutoff was selected beyond the distance of the first and the second solvation shells of K^+ ion each system). The cluster was then used as an input to the FEFF7 program [11–14], which calculates the EXAFS spectrum $\mu(E)$ for the probed ion as a function of energy, E, using a multiple scattering approach. Some configurations taken from each simulation were used to generate EXAFS spectra and then all spectra were averaged and compared to the measured one. Details of the MD-EXAFS method can also be found in our recent works [41–43].

Results

Swelling behavior for hydrated K^+-MMT

Before performing MD-EXAFS analysis, the molecular model for the hydrated K^+-MMT and the reliability of the force field used in this work were checked by a comparison of swelling behavior determined from XRD experiment. The interlayer spacing of hydrated K^+-MMT model was calculated as a function of water content (N_w = 0–150 molecules) and presented in Fig. 1. For the dried state (no water molecules in the interlayer), the simulation yields an interlayer spacing (D) of 9.9 Å which is close to 10.1 Å determined by the part reported X-ray diffraction experiment [46]. D is increased about 2 Å from N_w = 0–50. As $N_w > 50$, the arrangement of interlayer waters was changed from mono- to bi-layer pattern. For larger N_w, D is increased almost linearly, producing a transition from bi-layer to tri-layer pattern at N_w = 150. There is no plateau for the change of D from each multi-layer structure. These results are similar to those reported by Boek et al. [47] implying that using different clay models and simulation methods seem to be not much significant. Nevertheless, the difference seems reasonable taking into consideration the difference in force field definition, box size, and methodologies for calculation.

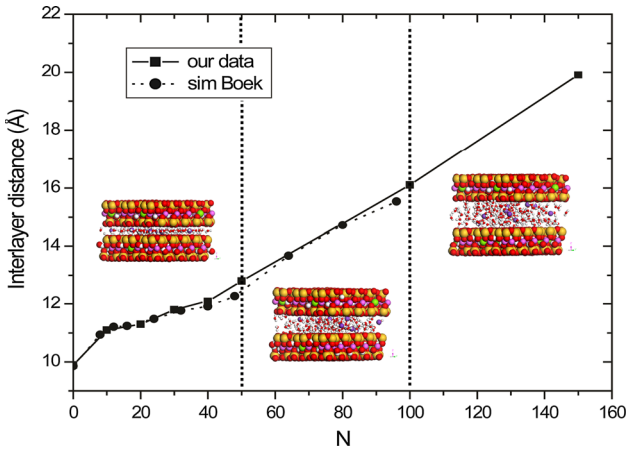

Fig. 1 Interlayer distance as a function of the number of water molecules. *Dot lines* are denoted to the region of mono-layer, bi-layer, and tri-layer hydrated K^+-MMT, respectively

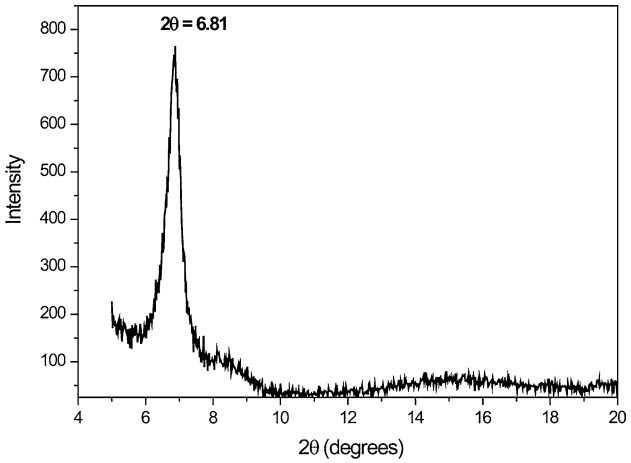

Fig. 2 X-ray diffractogram of hydrated K^+-MMT used in this work. The calculated interlayer spacing is 12.9 Å (2θ = 6.81°)."

Figure 2 presents X-ray diffractogram of hydrated K^+-MMT samples used in this work. The calculated interlayer

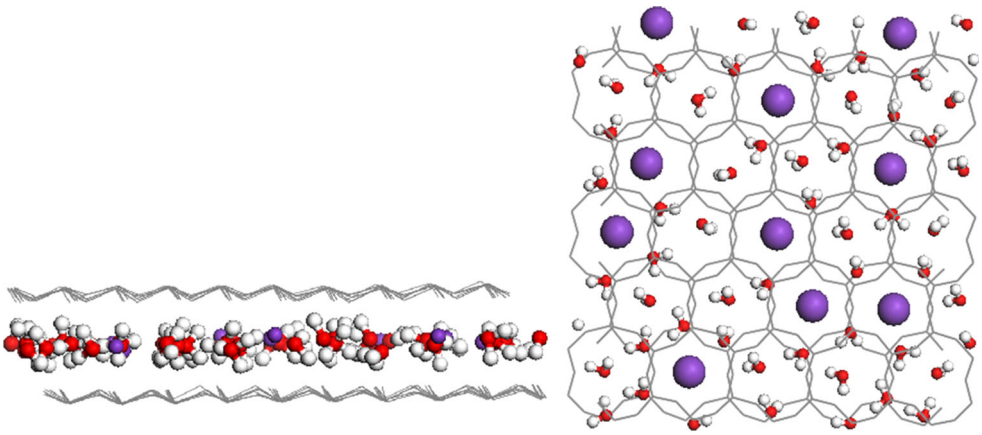

Fig. 3 A snapshot of an equilibrated system having 50 water molecules. (hydrogen, oxygen, and potassium are *white*, *red*, and *purple*, respectively) (Color figure online)

spacing is 12.9 Å ($2\theta = 6.81°$), which is equivalent to the simulation model of mono-layer hydrated K^+-MMT with $N_w = 50$. As illustrated in Fig. 3, the atomistic model of this mono-layer hydrated K^+-MMT shows that water molecules are strongly confined to a single layer at the midplane region along with the adsorbed counter K^+ ions. This mono-layer hydrated K^+-MMT model will then be employed to generate MD-EXAFS to investigate the structural properties of adsorbed K ions and interlayer species.

EXAFS and MD-EXAFS

Figure 4a, b presents the normalized, background-subtracted, and k^2-weighted EXAFS spectra $\chi(k)$ of K^+ ion adsorbed in the MMT and 1 mol/dm^3 KCl aqueous solution, respectively. In Fig. 4a, the k^2-weighted $\chi(k)$ experimental EXAFS and simulated MD-EXAFS spectra of monohydrated K^+-MMT are compared and an overall satisfactory agreement for both frequency and amplitude of oscillation over the k range from 1 to 8 Å^{-1} is clearly seen. Matching of the frequency of oscillation ensures that the K^+–O distances between experiment and simulation are almost the same. In comparison to K^+ ions in aqueous solution (Fig. 4b), the EXAFS signal for hydrated K^+-MMT has different oscillation patterns as the elements around the probed ion can be located at different distances with different coordination numbers. The corresponding $\tilde{\chi}(R)$ plots generated by Fourier transform of $k^2\chi(k)$ data are given in Fig. 5a, b, together with the computed generated ensemble MD-EXAFS. $\tilde{\chi}(R)$ represents the partial pair distribution functions convoluted with photoelectron scattering functions. There is a remarkably good agreement in the radial structures derived from experiment and simulation. A sample snapshot of the coordinated water oxygen atoms to K^+ ion in aqueous solution is presented in Fig. 6 (right). There are 7 water molecules surrounded with each K^+ ion, which is in good agreement with experimental EXAFS results and MD simulation with polarized

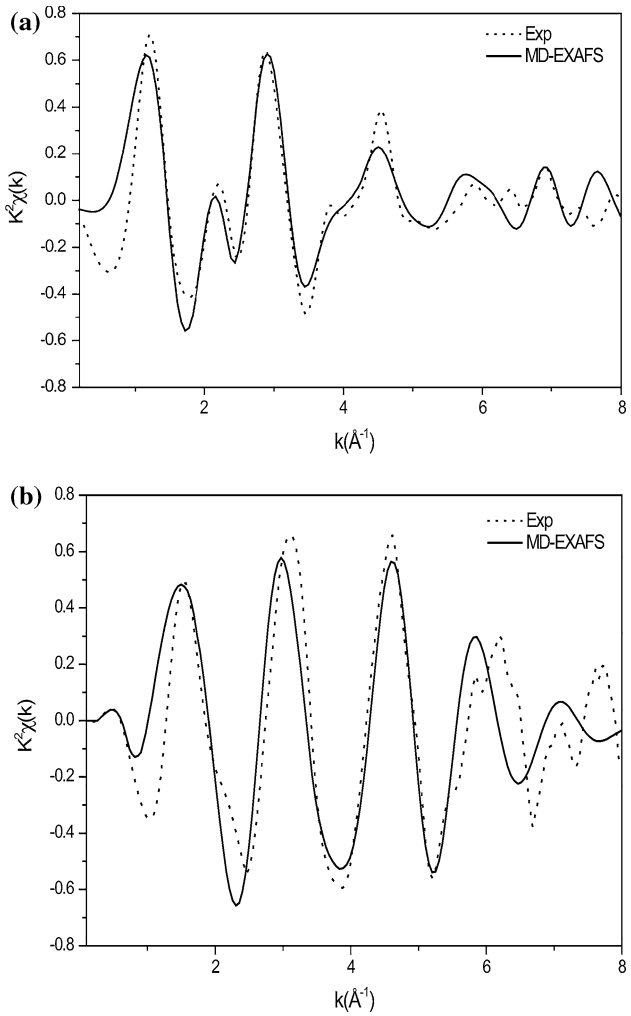

Fig. 4 A comparison between the simulated and experimental EXAFS k^2-weighted $\chi(k)$ plots for K^+ ion in **a** mono-layer hydrated K^+-MMT and **b** in aqueous solution

force field [19]. From Fig. 6 (left), there are two coordination shells for K^+ ions in mono-layer hydrated K^+-MMT, which is different from the situation in aqueous

solution. As commented earlier, this is due to the different environment around K^+ ions in the interlayer space of MMT. More details will be analyzed using the concept of the RDF in Section "Radial distribution function (RDF)."

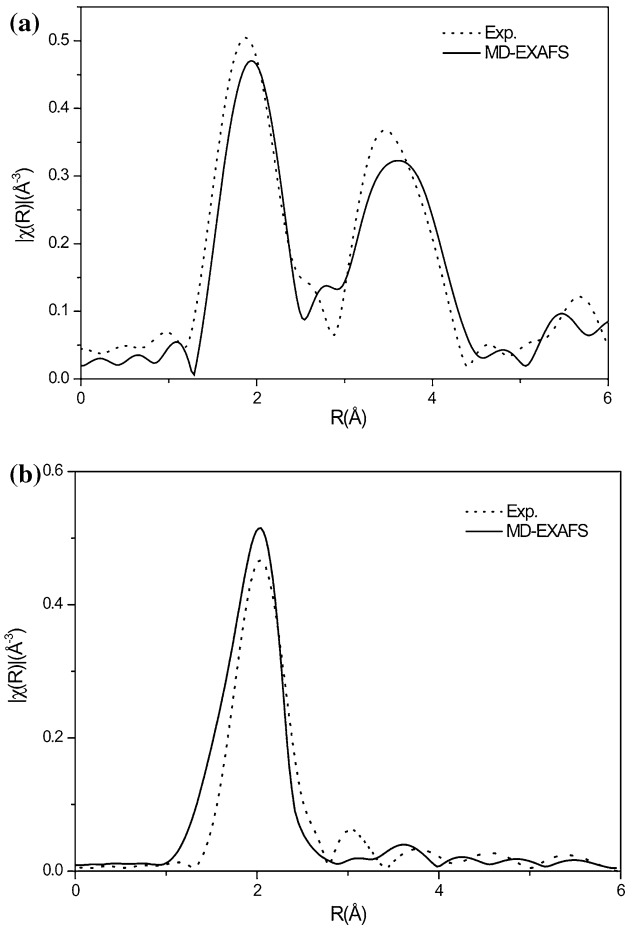

Fig. 5 A comparison between the simulated and experimental $|\tilde{\chi}(R)|$ plots corresponding to the Fourier transformed $k^2\chi(k)$ for K^+ ion **a** in mono-layer hydrated K^+-MMT and **b** in aqueous solution

The width of the $\tilde{\chi}(R)$ peak is concerned with the mean-squared displacement of the neighboring atoms and presented in Table 1 as the Debye–Waller factors (σ^2). This parameter is a measurement for the degree of configurational disorder of neighboring atoms around the K^+ ions. From the curve fitting, the Debye–Waller factor of the local structure around the K^+ ions in the clay interlayer (0.041) is larger than that in the aqueous solution (0.029). This indicates that water molecules are oriented more orderly in the first shell of K^+ ion in aqueous solution than those in the monohydrated K^+-MMT. The confinement effect from the narrow gap of MMT surface causes these interlayer waters to arrange with comparatively broader distribution of the mean-squared displacement of the neighboring atoms compared to those in the aqueous solution.

In addition, for the mono-layer hydrated clay, the Debye–Waller factor of the second shell (0.059) is larger than of the first shell (0.041) even though the counter K^+ ions interact with the rigid oxygen atoms from the MMT surface (O_{MMT}) which is expected to have more ordered configuration. It is anticipated that an increased disorder for molecular configuration in the second shell arises from the dynamics of K^+ ion relative to O_{MMT} while the arrangement of O_W around K^+ ion seems to have more ordered configuration in the first shell. Satisfactory agreement between EXAFS and MD simulation for the hydrated K^+-MMT convinces us that the MMT model and the PCFF-INTERFACE force field for clay and water used in this work are good enough to investigate other properties mainly by MD simulation.

In should be noted that the disorder contributing to the Debye–Waller factor can be considered as the result of two sources, the configurational disorder and the vibrational disorder [19]. The configurational disorder is determined from the MD simulation whereas vibrational contribution to the Debye–Waller factor can be estimated by quantum chemistry calculation. In this work, we focus only MD simulation to generated EXAFS spectra, and the vibrational

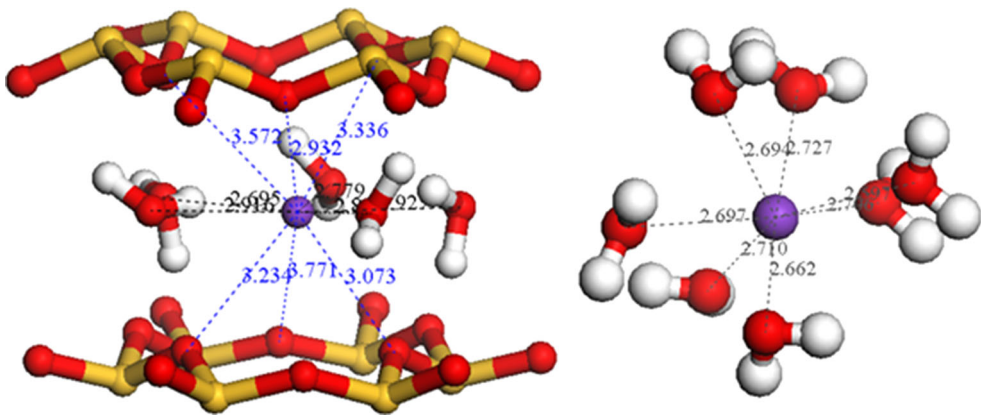

Fig. 6 Local environment around K^+ ion and its coordination shell, in the interlayer space of hydrated K^+-MMT (*left*) and aqueous solution (*right*). (hydrogen, oxygen, and potassium are *white*, *red*, and *purple*, respectively) (Color figure online)

Table 1 Parameters from EXAFS experiments

System	ΔE_0 (eV)	First shell (K–O_W)			Second shell (K–O_{MMT})		
		R(Å)	N	σ^2	R(Å)	N	σ^2
K^+ ions in aqueous solution	4.1	2.72	5.7	0.029	–	–	–
K^+ ions in hydrated MMT	4.8	2.81	5.4	0.041	3.66	6.1	0.059

ΔE_0 (eV) the difference between threshold energy in referent and sample spectra, R (Å) inter-atomic distances, N coordination number, σ^2 Debye–waller factor (Å^2)

contribution to the Debye–Waller factor was not corrected for quantum effects.

Density profiles

The density profiles for O, H, and K^+ in the interlayer space of hydrated K^+-MMT for $N_w = 50$, 100, and 150 are presented as the mono-, bi-, and tri-layer hydrates in Fig. 7a–c, respectively. The definition of mono-, bi-, and tri-layer hydrates is from the characteristics of density profile of interlayer species that show one, two, and three maxima (clearly seen for profiles of K^+ ions and oxygen water, O_W), respectively. For mono-layer hydrate, a high and narrow oxygen peak at the interlaminar midplane, two hydrogen peaks, symmetrically situated at both sides of the oxygen peak and a single potassium ion peak, also at the interlaminar midplane, are observed. Most of these results agree with the past report [30]. K^+ counter ions are distributed mainly near the midplane, but with a broader distribution about 0.5 Å from the midplane compared to O_W profile. These results indicate that K^+ ions can slightly move closer to the clay surface and form inner-sphere surface complexes that are not constrained to the small triangular region above two tetrahedral charge sites. Instead, they can move close to the basal-plane oxygen surrounding the charge sites. The profiles for water hydrogen (H_W) have two peaks pointed away from the midplane. About half of O–H bonds are pointed toward the clay surface because the partial charge of H_W is also positive (+0.40) like counter ions. An example snapshot that presents the arrangement of water molecules is previously given in Fig. 3. It seems that water molecules can be located anywhere on the clay surface which is different from the K^+ counter ions that need to be located at the adsorbed sites within the vicinity edge of a basal oxygen hexagonal cavity in the silicate tetrahedral sheets. This structure is different from those in monohydrated Na^+-MMT [10]. In the latter case, Na+ ions are distributed at the side of the oxygen peaks, closer to clay sheets and some of them are strongly attached to the clay surface to form inner-sphere surface complexes. This makes water molecules to cluster in two layers joined at the interlaminar midplane, producing an oxygen double peak. Naturally,

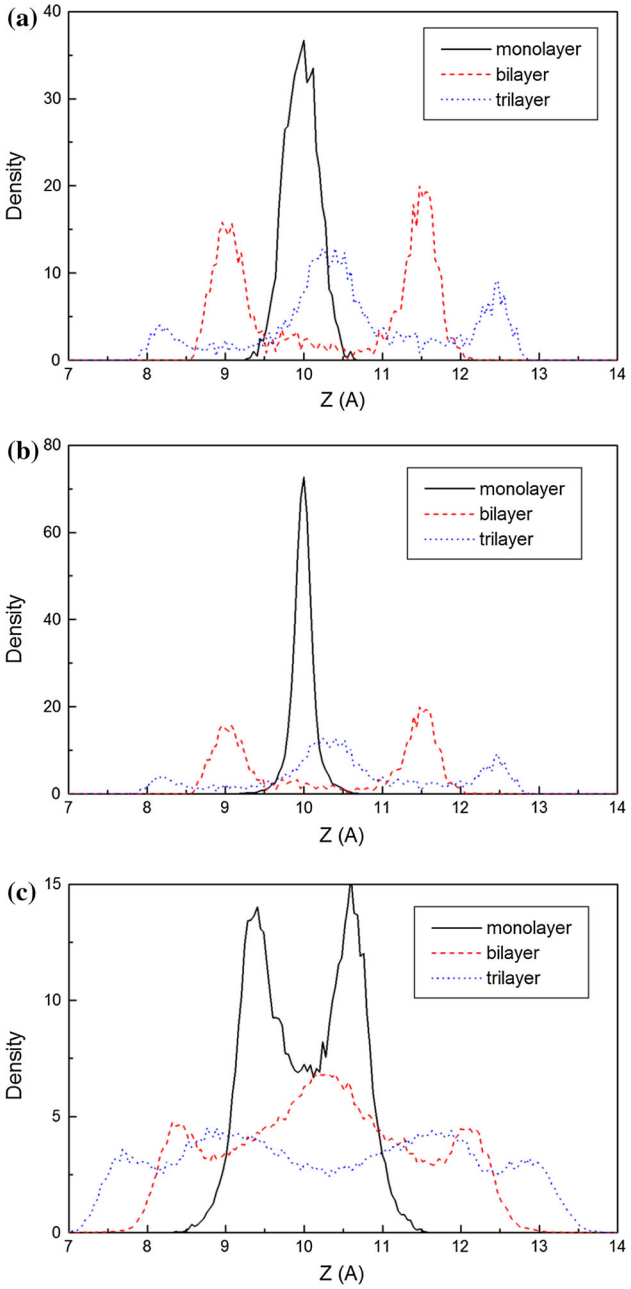

Fig. 7 Density profiles of the interlayer species for **a** K^+ ion **b** water oxygen (O_W) and water hydrogen (H_W) in mono-, bi- and tri-layer hydrated K^+-MMT. K^+, O_W, and H_W profiles are denoted by *solid*, *dash*, and *dot line*, respectively

this effect widens the interlaminar space, even though the size of sodium ion is smaller.

For bi- and tri-layer hydrate, the counter ion density profiles shown in Fig. 7a indicate that K^+ ions prefer to stay closer to the clay surface with small amplitude of density in the diffuse-layer region. On the other hand, the highest peak of the counter ion density profiles for tri-layer hydrates is seen at the midplane region with two smaller peaks near the clay surface. The profiles for water oxygen and hydrogen exhibit similar characteristics as seen in Fig. 7b, c. These results indicate that the K^+ ions can form surface complexes that are inner-sphere, outer-sphere, and transient diffuse-layer species depending on the number of intercalated water in the clay.

Radial distribution function (RDF)

Radial distribution functions (RDFs) from MD simulation give a quantitative analysis of the atomistic local structure such as the averaged distance between the probed atom and its neighboring atom (R) and coordination number (N). However, it is important to note that these RDFs are not exactly the same as $\tilde{\chi}(R)$ determined from experimental EXAFS [11–14]. From Fig. 8 and Table 2, the first (and second) K^+–O peaks from MD simulation are located at 2.69 (6.3) and 2.85 (3.7) Å for K^+ ions in aqueous solution and mono-layer hydrated K^+-MMT, respectively. For K^+ in aqueous solution, the first peak of K–O RDF centered at 2.69 Å with $N = 6.3$ is in good agreement with ab initio dynamic results (2.80 Å and 6.0–6.8) [17]. For the hydrated clay system, a wider separation ($R = 2.85$ Å, $N = 3.73$) is seen for the K^+–O_W distance as a consequence of confinement that pushes water molecules at the midplane region away from others in parallel direction to the clay surface. This confinement effect also causes smaller N for the first and second shell of K^+-O peaks in the clay system although K^+-O distances are larger. The K^+-O coordination numbers are somewhat inflated in aqueous system due to smaller separation of the O–O sites (2.75 vs. 2.93 Å in Fig. 8b) that cause water molecules to have denser configuration in the hydrated K^+-MMT. Large contribution from clay can influence this coordination number as K^+ ions can interact with both clay layers simultaneously and hold the sheets together. From Fig. 8a, K^+ ions are practically centered at the interlayer midplane, K^+–O_{MMT} distance = 3.41 Å, and appear as a broader peak (from 3.0 to 4.5 Å) compared to that of K^+–O_W (from 2.5 to 3.5 Å) with an average of 5.1 O_W and 5.8 O_{MMT} surrounding each K^+ ion which tend to separate from each other. No water molecule is interposed between these counter ions and clay sheet. For mono-layer hydrated MMT, K^+ ions can behave as inner-sphere complexes and interact simultaneously with both clay layers as illustrated in Fig. 6 (left). There are about 5 O_W and 6 O_{MMT}

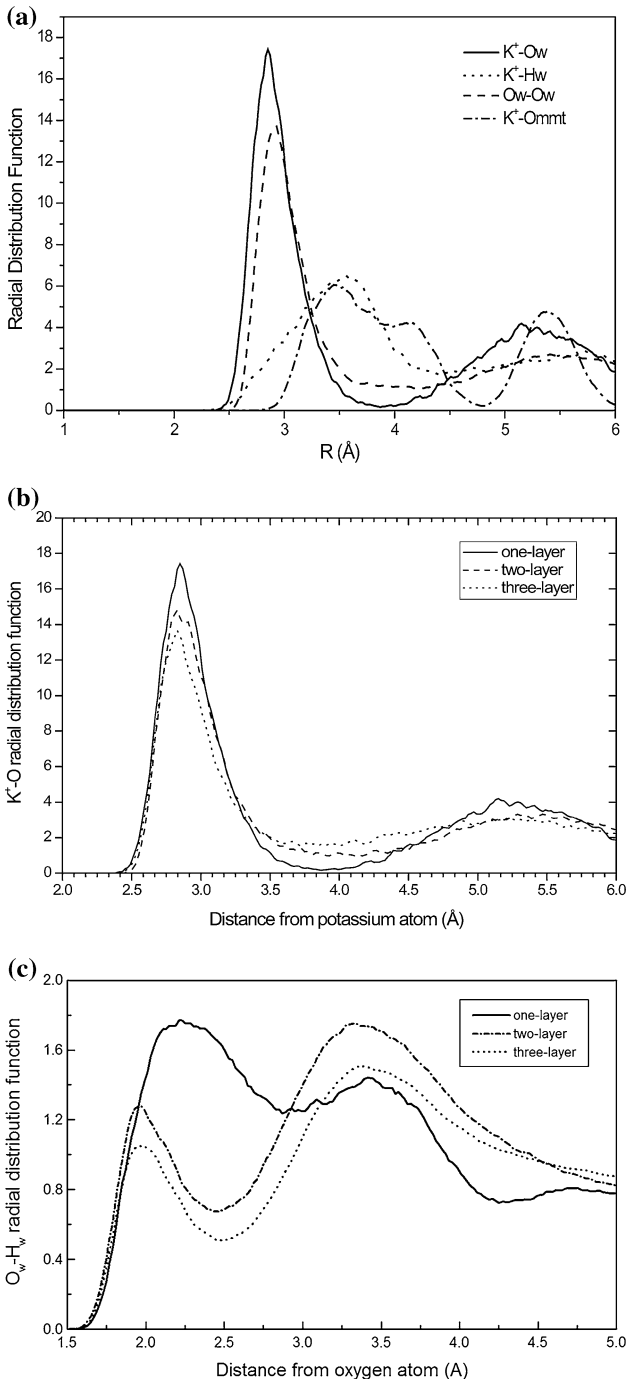

Fig. 8 **a** Radial distribution functions (RDFs) for $K^+ - O_W$, $K^+ - H_W$, $O_W - O_W$ and $K^+ - O_{MMT}$ in monohydrated K^+-MMT **b** The K-O_W RDF for interlayer water molecules in three hydrated K^+-MMT and **c** the O_W-H_W RDF for interlayer water molecules in three hydrated K^+-MMT

from each clay layer surrounded K^+ ion at the average distance of 2.81 and 3.41 Å, respectively. The K^+ counter ions appear to be attracted toward the two tetrahedral charge sites, but the counter ions are not constrained to the small triangular region above these sites as evidenced from the

Table 2 Structural parameters derived from MD simulation

System	$K^+ - O_{H_2O}$		$K^+ - H_{H_2O}$		$O_{H_2O} - O_{H_2O}$		$K^+ - O_{MMT}$	
	R (Å)	*N*	*R* (Å)	*N*	*R* (Å)	*N*	*R* (Å)	*N*
Aqueous	2.69	6.30	3.33	20.40	2.75	4.80	–	–
	(2.80)[a]	(6.00–6.80)[a]	(3.30)[a]	(20.0)[a]	(2.70)[a]	(4.50)[a]	–	–
MMT	2.85	5.10	3.73	8.20	2.93	3.00	3.41	5.80
	(2.80)[b]				(2.90)[b]			

[a] ab initio dynamics simulations [27]

[b] MCY model estimates based on MD simulation [40]

broad peak of K^+–O_{MMT} RDF from 3.0 to 4.5 Å. Accordingly, the K+ counter ions should move close to the basal-plane oxygen ions surrounding the charge sites and appear to be forming inner-sphere surface complexes with ditrigonal cavities.

For bi- and tri-layer hydrates, the peaks of RDFs are located at 2.83 and 3.31 Å for K–O_W and K–O_{MMT}, respectively. The K–O_{MMT} distance is slightly decreased about 0.10 Å compared to the single layer hydrated MMT and this distance is different for clay with $N_W < 100$, suggesting that this value should be the natural average K–O distance for K^+ attached to the siloxane surface. For tri-layer hydrate, the corresponding coordination numbers are 6.9 and 2.9 for water and clay, respectively. The coordination number is much lower for the tri-layer hydrated MMT than that for the single and double layers hydrated MMT. This is because the potassium ions can be coordinated to only one MMT plane. As expected, the K–O_W coordination numbers increase with the number of water molecules, whereas K–O_{MMT} coordination numbers decrease. The main peak in the O–O RDF (Fig. 8b) occurs at 2.93 Å in the one-layer hydrated MMT and at 2.75 Å in the two- and three-layer hydrated MMT. The sharpness of the first peak in the RDF suggests that water molecules near the midplane (m) in the three-layer hydrated MMT are more organized, whereas the breadth of the first peak in the RDF suggests the opposite for water molecules in the one-layer hydrated MMT.

From Fig. 8c, the O_W–H_W RDF peaks indicate that hydrogen bonds are stretched significantly in the one-layer hydrate (2.25 vs. 1.95 Å in higher-layer hydrates) while the next-nearest neighbor O–H distances (3.45 vs. 3.55 Å for mono- and higher-layer hydrates, respectively) are quite similar in all three hydrates indicating hydrogen bonds are bent somewhat.

Interlayer species mobility

In general, EXAFS is not an experimental method to investigate the dynamic properties of elements. The information of the local structure around the probed species is determined by an ensemble average of atomic coordinates from all elements that move within a small distance near the probed species. Therefore, only the results of some dynamic properties of interlayer species by MD simulation are presented here.

The self-diffusion coefficient of water molecules (D_W) and K^+ ion (D_k) in mono-layer hydrated MMT was estimated by MD simulation as 2.10×10^{-10} and 6.0×10^{-11} m^2s^{-1}, respectively. These values are in similar magnitude and trend with MD simulation of MCY model (1.3×10^{-10} and 1.2×10^{-10} m^2s^{-1}) [48]. D_K and D_W for the single layer hydrated MMT are clearly less than that in aqueous solution. There are no reported D_K values for lower-order hydrated K^+-MMT. K^+ ions move very little mostly in the parallel direction to the MMT surface (for 1 ns simulation, the ratio of the mean square displacement for the parallel direction is about 3 times to the normal direction to the clay surface). The negative charges on MMT surface retard the motions of K^+. K^+ ions in the single layer hydrates are almost trapped within the cavities of the basal planes' surface complexes near tetrahedral charge sites.

Conclusions

The interlayer space distance of K^+-MMT as the function of water content was determined by the MD simulations. Most results from the *NPT* simulations were consistent with those previously reported indicating that difference in simulation models and methods is not significant. Subsequently, MD-simulated EXAFS spectra were calculated and were in satisfactory agreement with the corresponding EXAFS experimental measurement. Based on the results derived from MD simulations and MD-EXAFS, the coordination number of water-solvated potassium at room temperature is about 7 and the K–O average distance is 2.69 Å for aqueous solution system. For the hydrated K^+-MMT, the first- and the second-neighbor back-scattered atoms derived from EXAFS analyses are presumed to be oxygen atoms from the interlayer water and oxygen atoms from MMT surface. There are about 5 water molecules

surrounded K^+ ion and additional 6 oxygen atoms from each closest silicates tetrahedral sheet. The MD-EXAFS results indicate that the adsorbed K^+ ions are located near the vicinity edge of the basal oxygen hexagonal cavity in the silicate tetrahedral sheets. For monohydrated MMT, K^+ counter ions are confined at the interlayer midplane region and form inner-sphere complexes simultaneously with both silicate layers with no water molecules interposed. For higher-layer hydrated MMT, K^+ ions can form surface complexes that are inner-sphere, outer-sphere, and transient diffuse-layer species depending on the number of intercalated water in the clay. Compared to higher-layer hydrates, water molecules are of less ordered arrangement in the monohydrated MMT due to the confinement effect from the clay surface. K^+ counter ions in the single layer hydrates are almost trapped within the cavities of the basal planes surface. The dynamics of interlayer species are increased for higher-layer hydrates. The comparison also shows that the performance of the force field in MD is just as good as results by ab initio calculation. Thereby, classical MD requires only a fraction of the computational cost, and ab initio MD itself can have significant uncertainties depending on the density functional chosen.

Acknowledgements This work was supported by the Thailand Research Fund under TRF Senior Research Scholar program Grant No. RTA568002. We thank Synchrotron Light Research Institute (Public Organization) for support on X-ray Absorption experiment and National Nanotechnology Center for permission to use Material Studio software.

References

1. Sposito G (1984) The surface chemistry of soils. Oxford University Press, New York
2. Velde B (1995) Origin and mineralogy of clays. Springer, New York
3. Grim RE (1962) Applied clay mineralogy. McGraw-Hill, New York
4. Teng BKG (1974) The chemistry of clay: organic reactions. Wiley, New York
5. Heinz H (2012) Clay minerals for nanocomposites and biotechnology: surface modification, dynamics and responses to stimuli. Clay Miner 47:205–230
6. Singh B, Ishwarya G, Gupta M, Bhattacharyya SK (2015) Geopolymer concrete: a review of some recent developments. Constr Build Mater 85:78–90
7. Giannelis EP (1996) Polymer layered silicate nanocomposites. Adv Mater 8:29–35
8. Lebaron PC, Wang Z, Pinnavaia T (1999) Polymer-layered silicate nanocomposites: an overview. J Appl Clay Sci 15:11–29
9. Alexandre A, Dubois P (2000) Polymer-layered silicate nanocomposites: preparation, properties and uses. Mater Sci Eng 28:1–63
10. Greenwell HC, Jones W, Coveney PV, Stackhouse S (2006) On the application of computer simulation techniques to anionic and cationic clays: a materials chemistry perspective. J Mater Chem 16:708–723
11. Rehr JJ, Albers RC (1990) Scattering-matrix formulation of curved-wave multiple-scattering theory: application to X-ray-absorption fine structure. Phys Rev B 41:8139–8149
12. Rehr JJ, Mustre de Leon J, Zabinsky SI, Albers RC (1991) Theoretical X-ray absorption fine structure standards. J Am Chem Soc 113:5135–5140
13. Rehr JJ, Albers RC, Zabinsky SI (1992) High-order multiple-scattering calculations of X-ray-absorption fine structure. Phys Rev Lett 69:3397–3400
14. Zabinsky SI, Rehr JJ, Ankudinov A, Albers RC, Eller MJ (1995) Multiple-scattering calculations of x-ray-absorption spectra. Phys Rev B 52:2995–3009
15. Newville M, Ravel B, Haskel D, Rehr JJ, Stern EA, Yacoby Y (1995) Analysis of multiple-scattering XAFS data using theoretical standards. Phys B 209:154–156
16. Ferlat G, San Miguel A, Jal JF, Soetens JC, Bopp PA, Daniel I, Guillot S, Hazemann JL, Argoud R (2001) Hydration of the bromine ion in a supercritical 1:1 aqueous electrolyte. Phys Rev B 63:134202–134211
17. Fulton JL, Heald SM, Badyal YS, Simonson JM (2003) Understanding the effects of concentration on the solvation structure of Ca^{2+} in aqueous solution. I: the perspective on local structure from EXAFS and XANES. J Phys Chem A 107:4688–4696
18. Ravel B, Newville M (2005) ATHENA, ARTEMIS, HEPHAESTUS: data analysis for X-ray absorption spectroscopy using *IFEFFIT*. J. Synchrotron Radiat 12:537–541
19. Glezakou VA, Chen Y, Fulton JL, Schenter GK, Dang LX (2006) Electronic structure, statistical mechanical simulations, and EXAFS spectroscopy of aqueous potassium. Theor Chem Acc 115:86–99
20. Corker JM, Evans J, Rummey JM (1991) EXAFS studies of pillared clay catalysts. Mater Chem Phys 29:201–209
21. Sylwester ER, Hudson EA, Allen G (2000) The structure of uranium (VI) sorption complexes on silica, alumina, and montmorillonite. Geochim Cosmochimica Acta 64:2431–2438
22. Scheckel KG, Sparks DL (2000) Kinetics of the formation and dissolution of Ni precipitates in a gibbsite/amorphous silica mixture. J Colloid Interface Sci 229:222–229
23. Cole T, Bidoglio G, Soupioni M, O'Gorman GN (2000) Diffusion mechanisms of multiple strontium species in clay. Geochim Cosmochim Acta 64:385–396
24. Ford RG, Sparks DL (2000) The nature of Zn precipitates formed in the presence of pyrophyllite. Environ Sci Technol 34:2479–2483
25. Zhang PC, Brady PT, Arthur SE, Zhou WQ, Sawyer D, Hesterberg DA (2001) Adsorption of barium(II) on montmorillonite: an EXAFS study. Colloids Surf A 190:239–249
26. Hesterberg D, Sayer DE, Zhou W, Rbarge WP, Plummer GM (1997) XAFS characterization of copper in model aqueous systems of humic acid and illite. J Phys IV 7:833–834
27. Nakano M, Kawamura K, Ichikawa Y (2003) Local structural information of Cs in smectite hydrates by means of an EXAFS study and molecular dynamics simulations. Appl Clay Sci 23:15–23
28. Skipper NT, Chang FRC, Sposito G (1995) Monte Carlo simulation of interlayer molecular structure in swelling clay minerals 1: methodologies. Clays Clay Miner 43:285–293
29. Chang FRC, Skipper NT, Sposito G (1995) Computer simulation of interlayer molecular structure in sodium montmorillonite hydrates. Langmuir 11(1995):2734–2741
30. Chang FRC, Skipper NT, Sposito G (1998) Monte Carlo and molecular dynamics simulations of electrical double-layer structure in potassium-montmorillonite hydrates. Langmuir 114:1201–1207
31. He HP, Galy J, Gerard JF (2005) Molecular simulation of the interlayer structure and the mobility of alkyl chains in HDTMA+/montmorillonite hybrids. J Phys Chem B 109:13301–13306
32. Chavez-Paez M, Van Workum K, De Pablo L, De Pablo JJ (2001) Monte Carlo simulations of Wyoming sodium montmorillonite hydrates. J Chem Phys 114:1405–1413

33. D'Angelo P, Di Nola A, Filipponi A, Pavel NV, Roccatano D (1994) An extended x-ray absorption fine structure study of aqueous solutions by employing molecular dynamics simulations. J Chem Phys 100:985–994
34. McCarthy MI, Schenter GK, Chacon-Taylor MR, Rehr JJ, Brown GE (1997) Prediction of extended x-ray-absorption fine-structure spectra from molecular interaction models: $Na^{+}(H_2O)_n$–MgO(100) interface. Phys Rev B 56:9925–9936
35. Wallen SL, Palmer BJ, Pfund DM, Fulton JL, Newville M, Ma Y, Stern EA (1997) Hydration of bromide ion in supercritical water: an X-ray absorption fine structure and molecular dynamics study. J Phys Chem A 101:9632–9640
36. Roccatano D, Berendsen HJC, D'Angelo PJ (1998) Assessment of the validity of intermolecular potential models used in molecular dynamics simulations by extended x-ray absorption fine structure spectroscopy: a case study of Sr^{2+} in methanol solution. J Chem Phys 108:9487–9497
37. Wallen SL, Palmer BJ, Fulton JL (1998) The ion pairing and hydration structure of Ni^{2+} in supercritical water at 425 °C determined by x-ray absorption fine structure and molecular dynamics studies. J Chem Phys 108:4039–4046
38. Hoffmann MM, Darab JG, Palmer BJ, Fulton JL (1999) A transition in the Ni^{2+} complex structure from six- to four-coordinate upon formation of ion pair species in supercritical water: an X-ray absorption fine structure, near-infrared, and molecular dynamics study. J Phys Chem A 103:8471–8482
39. Fulton JL, Hoffmann MM, Darab JG, Palmer BJ, Stern EA (2000) Copper(I) and copper(II) coordination structure under hydrothermal conditions at 325 °C: an X-ray absorption fine structure and molecular dynamics study. J Phys Chem A 104:11651–11663
40. Spangberg D, Hermansson K, Lindqvist-Reis P, Jalilehvand F, Sandstrom M, Persson I (2000) Model extended X-ray absorption fine structure (EXAFS) spectra from molecular dynamics data for Ca^{2+} and Al^{3+} aqueous solutions. J Phys Chem B 104:10467–10472
41. Merat K, Chaodamrongsakul J, Tanthanuch W, Vao-soongnern V (2013) A combined molecular dynamic simulation and X-ray absorption spectroscopy to investigate the atomistic solvation structure of cation in poly(vinyl alcohol):potassium thiocyanate (KSCN) solid electrolytes. J Non-Crystalline Solids 371–372: 47–52
42. Chaodamrongsakul J, Merat K, Klysubun W, Vao-soongnern V (2013) A combined molecular dynamic simulation and X-ray absorption spectroscopy to investigate the atomistic solvation structure of cation in poly(vinyl alcohol):potassium thiocyanate (KSCN) solid electrolytes. J Non-Crystalline Solids 379:21–26
43. Chaodamrongsakul J, Klysubun W, Vao-soongnern V (2014) Application of X-ray absorption spectroscopy and molecular dynamics simulation to study the atomistic solvation structure of tetraglyme:KSCN electrolytes. Mater Chem Phys 143:1508–1516
44. Heinz H, Koerner H, Anderson KL, Vaia RA, Farmer BL (2005) Force field for mica-type silicates and dynamics of octadecylammonium chains grafted to montmorillonite. Chem Mater 17:5658–5669
45. Heinz H, Lin TJ, Mishra RK, Emami FS (2013) Thermodynamically consistent force fields for the assembly of inorganic, organic, and biological nanostructures: the INTERFACE force field. Langmuir 29:1754–1765
46. Calvet R (1973) Hydratation de la montmorillonite et diffusion des cations compensateurs-I: Etude de l'hydra-tation de la montmorillonite saturee par des cations monovalents. Ann Agron 24:77–133
47. Boek ES, Coveney PV, Skipper NT (1995) Monte Carlo molecular modeling studies of hydrated Li-, Na-, and K-smectites: understanding the role of potassium as a clay swelling inhibitor. J Am Chem Soc 117:12608–12617
48. Cebula DJ, Thomas RK, White JW (1980) Small angle neutron scattering from dilute aqueous dispersions of clay. J Chem Soc, Faraday Trans 76:314–321